Hindawi
Journal of Electrical and Computer Engineering
Volume 2020, Article ID 1959073, 9 pages
https://doi.org/10.1155/2020/1959073

Research Article

Research on Adaptive Suppression of LCL Converter Resonance Grid-Connected System

Junwei Li,[1,2] **Yafang Tang**,[2] **and Junke Li**[1]

[1]*Qiannan Normal University for Nationalities, Duyun, Guizhou 558000, China*
[2]*School of Electrical Engineering, Guizhou University, Guiyang, Guizhou 550025, China*

Correspondence should be addressed to Yafang Tang; 1560368@qq.com and Junke Li; 125850238@qq.com

Received 5 October 2019; Revised 11 December 2019; Accepted 17 March 2020; Published 28 April 2020

Academic Editor: Amir Sabbagh Molahosseini

LCL-type converters are widely used in grid-connected systems due to their small size and good filtering performance. However, the resonance suppression problem brought by the LCL filter cannot be ignored. The capacitive current feedback is a commonly used resonance suppression method. In applications, the grid impedance can cause LCL filter resonance. Thus, this paper presents an adaptive resonance suppression method based on the RBF network optimized by particle swarm optimization. This method optimizes the initial parameters of the RBF network through particle swarm optimization, identifies the parameters of the PI controller by RBF neural network's own identification capability, and updates the active damping coefficient based on constraints such as stability margin, thereby realizing the LCL-type inverter to maintain the system stability when the grid impedance changes. The effectiveness of the method is verified by experiments.

1. Introduction

Renewable energy based distributed power generation system (RE-DPGS), as an efficient and highly promising power generation method, plays an important role in modern power grid systems [1]. As a power interaction device between the renewable energy power generation system and the smart grid, the LCL converter plays a pivotal role in the modern smart grid [2]. However, as the LCL filter is a third-order system, its own resonant peak is also a key factor threatening the stability of the grid-connected converter system [3, 4]. Therefore, the research on the suppression of LCL converter resonance has practical significance for improving the system's operating efficiency and reliability.

At present, a great number of studies have been conducted on the methods of suppressing the harmonic resonance of LCL-type inverter, including passive damping and active damping methods [5, 6]. Passive damping is worked by connecting the LCL filter capacitor in parallel or in series with a damping resistor to achieve resonance suppression. Compared with the passive damping method, the active damping method uses an optimized control method to solve the resonance problem of the LCL converter, can avoid additional power loss, and is widely used in medium and high power converter systems. Active damping mainly includes the state feedback method [7], notch-based damping control method [8], and harmonic current extraction technique-based damping method [9].

The commonly used controllers in the grid-connected converter control strategy are the PR controller [10], PI controller [11], repeated control [12], and fuzzy control and hysteresis control [13]. The PR controller can suppress the grid harmonics effectively, but when the harmonic frequency of the grid approaches the cut-off frequency of the system, the PR controller will reduce the phase angle margin of the system and cause system instability. The PI controller can improve the steady-state performance of the system and suppress harmonics which is smaller than the cut-off frequency f_c and ensure that there is no steady-state error adjustment to achieve stable operation of the grid system. The accuracy of hysteresis control is affected by the loop width and switching frequency. Fuzzy control rules are based on experience, and the system's steady-state tracking

ability is poor. Repetitive control works based on the intimal principle and the dynamic characteristics of the system affected by the intimal are poor. However, no matter which kind of controller is used, its parameters are designed under the standard condition, and the high accuracy of the system model is required. When the impedance of the grid changes, it will affect the steady-state error of the system and the power quality of the grid-connected system.

This paper presents a resonance suppression strategy based on particle swarm optimization to optimize the RBF neural network and closed-loop parameter design method for LCL-type grid-connected inverter. According to the change of grid impedance, this strategy can set appropriate PI controller parameters through the recognition ability of RBF neural network and get the relationship capacitor current feedback coefficient with constraints of phase angle margin, amplitude margin, and system damping ratio, so as to calculate the optimal feedback coefficient of the PI controller parameter. It is verified based on the SIMULINK simulation platform.

2. LCL-Type Inverter Mathematical Model

The control structure of the single-phase grid-connected converter is shown in Figure 1. The DC power supply u_d is the inverter input; C_{dc} is the DC side capacitor; i_{inv} is the inverter output current; u_{inv} is the inverter output voltage; C is the filter; u_c is the filter capacitor voltage; L_1 is the inverter side inductor; L_2 is the grid side inductor; i_c is the capacitor current, i_g is the grid-connected current; u_g is the grid voltage; the switching device is a symmetrical switch bridge arm. The device is an ideal device.

The grid-connected converter control strategy shown in Figure 1 is as follows. The error value between grid-connected current and reference current containing grid phase and frequency information, through controller and pulse width modulation strategy (SPWM) module, generates the modulation pulse to control the power switch on and off. This can make the output current of the grid-connected converter have the same phase information with the grid voltage and ensure that the THD of the output current of the grid-connected converter meets the grid-connected standard. According to the electrical attribute relationship between the various components, the control block diagram of the single-phase grid-connected converter can be obtained, as shown in Figure 2.

The open-loop transfer function of the grid-connected system is

$$G_O(s) = \frac{G_{PI}K_{pwm}}{s^3L_1L_2C + s^2L_2CH_{i1}K_{pwm} + s(L_1 + L_2)}. \quad (1)$$

3. Resonance Analysis

3.1. LCL Grid-Connected Converter Resonance Analysis. The analysis in this paper only involves higher harmonics, and the ideal grid voltage only works at the fundamental voltage. Therefore, this paper only considers the grid voltage

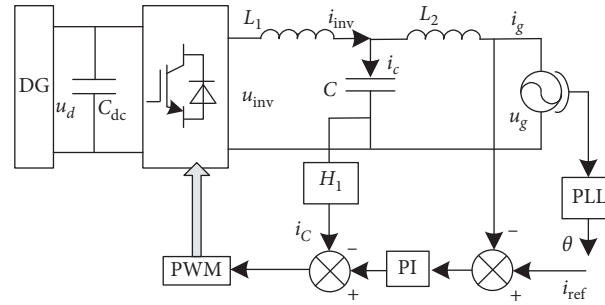

Figure 1: Control structure of the grid-connected converter.

as the influence of the disturbance. The transfer function of u_{inv} to grid-connected current i_g from Figure 1 is

$$Y(s) = \frac{i_g(s)}{u_{inv}(s)} = \frac{1}{s[s^2L_1L_2C + (L_1 + L_2)]}. \quad (2)$$

It can be seen from the above equation that the resonant angular frequency of the LCL filter is

$$\omega_0 = \sqrt{\frac{L_1 + L_2}{L_1L_2C}}. \quad (3)$$

3.2. Considering the Resonance Analysis of Grid-Connected System under Grid Impedance. In the grid-connected system, the magnitude of the grid impedance can affect the work performance of the LCL filter. The grid impedance is mainly inductive, which is expressed by L_g. The grid-connected current is affected by L_G which is the sum of the grid side inductance and the grid impedance ($L_G = L_2 + L_g$), so that the transfer function of u_{inv} to grid-connected current i_g is

$$Y(s) = \frac{i_g(s)}{u_{inv}(s)} = \frac{1}{s[s^2L_1CL_G + (L_1 + L_G)]}. \quad (4)$$

Then, the resonant frequency of the transfer function is

$$\omega_r = \frac{1}{\sqrt{C \bullet L_1 \bullet (L_2 + L_g)/(L_1 + L_2 + L_g)}}. \quad (5)$$

Figure 3 shows the Bode plot of the transfer function $Y(s)$ considering the grid impedance and the ideal grid impedance, respectively. The filter parameters are shown in Table 1.

It can be seen from Figure 3 that as the grid impedance becomes larger, the system resonance changes. The LCL filter has a resonance peak at the frequency ω_{r1} and ω_{r2}, and the phase information in both cases is traversed by $-\pi$ in the negative direction. According to the control theory, the negative crossing will generate a closed-loop pole in the right half plane, which will cause the unstable operation of the grid-connected converter system. After considering L_g, the resonant angular frequency of the inverter grid-connected system will move to the low-frequency band. Obviously, it is difficult to maintain stability without the damping suppression resonance.

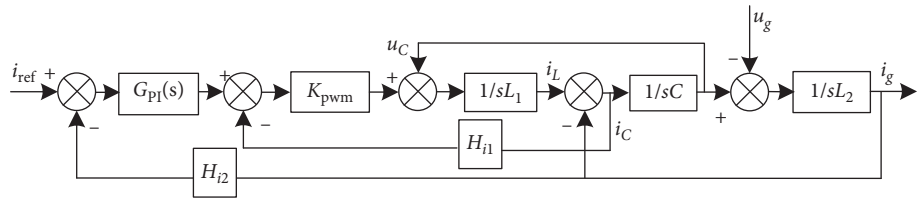

Figure 2: Block diagram of the control system of the single-phase grid-connected converter.

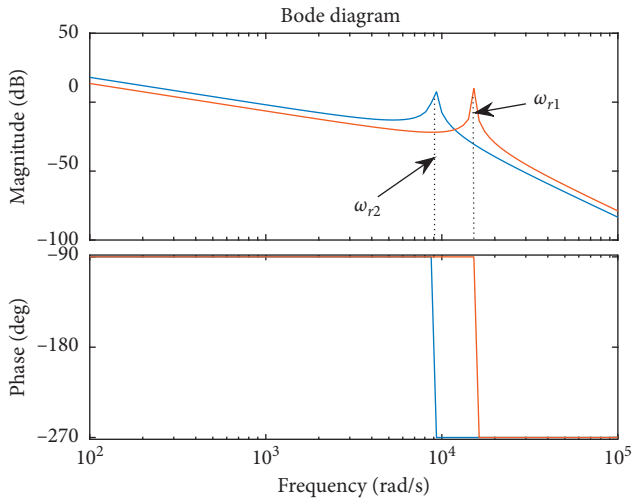

Figure 3: Bode diagram of the transfer function $Y(s)$.

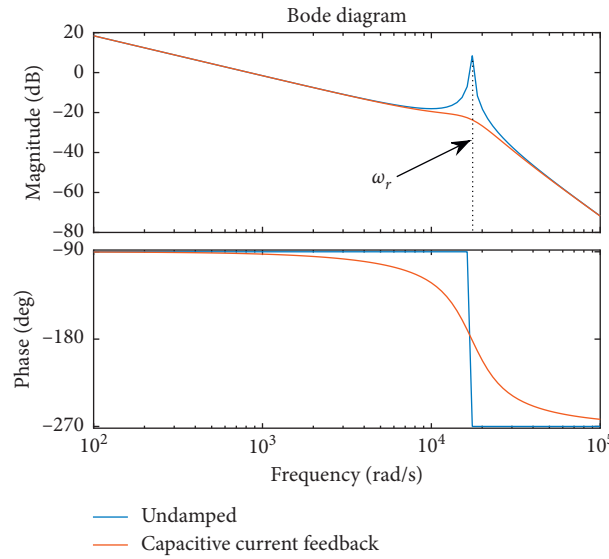

Figure 4: Capacitive current feedback damping.

Table 1: Grid system parameters.

System parameters	Value
Converter side inductance (mH)	1
Grid side inductance (mH)	0.2
Filter capacitor (μF)	20
Fundamental frequency (Hz)	50
Switch frequency (kHz)	10
Inverter output power (kW)	3.7
Learning rate (η)	0.2
Momentum factor (∂c)	0.1
DC side voltage (V)	400
Power voltage (V)	220
Grid inductance (mH)	1

4. Strategy Analysis

4.1. Capacitive Current Feedback Active Damping. Capacitive current feedback active damping uses a control method to modify the resonant frequency characteristics of the LCL filter. As shown in Figure 4, this method can effectively suppress resonance spikes without reducing the low-frequency gain and high-frequency harmonic attenuation of the LCL filter and increasing the extra power loss of the system.

4.2. Selecting the Capacitor Current Feedback Coefficient. The PI controller can reduce the current harmonics at the grid-connected point and improve the quality of the grid-connected power. The selection of the appropriate capacitor current feedback coefficient in the stable operation of the grid-connected system is greatly affected by the PI controller parameters and the stability margin of the system [14]. So, H_{i1} design can be summarized as follows. According to the relationship between the amplitude margin G_M of the grid-connected converter, the phase margin P_M, and H_{i1}, K_p, K_i, we calculated the range of H_{i1} and determined the optimal value. Next, the relationship between H_{i1}, K_p, K_i, and P_M, G_M is analysed in detail. The parameters used in the calculation are shown in Table 1.

When using capacitor current compensation, different compensation coefficients have different suppression effects on resonance [5]. When the H_{i1} value is large, it has a better damping effect on the resonance frequency f_r and hardly affects the amplitude-frequency characteristics of the high-frequency and low-frequency bands; as the H_{i1} value increases, the phase angular margin becomes smaller. Therefore, selecting various H_{i1} values can affect the phase angle margin and amplitude margin of the grid-connected system.

Figure 5 shows the inner loop Bode diagram of the grid-connected system when K_p and K_i take different parameters. First, the K_i parameter is fixed and the K_p parameter is adjusted; then, the K_p parameter is fixed and the K_i parameter is adjusted. It can be seen that as the K_p parameter increases, the phase angle margin increased and the amplitude margin reduced; while setting the larger value of the K_i parameter, the phase margin reduced, and there is almost no effect on the amplitude margin. Therefore, when calculating the amplitude margin, the PI controller can be regarded as the K_p proportional controller.

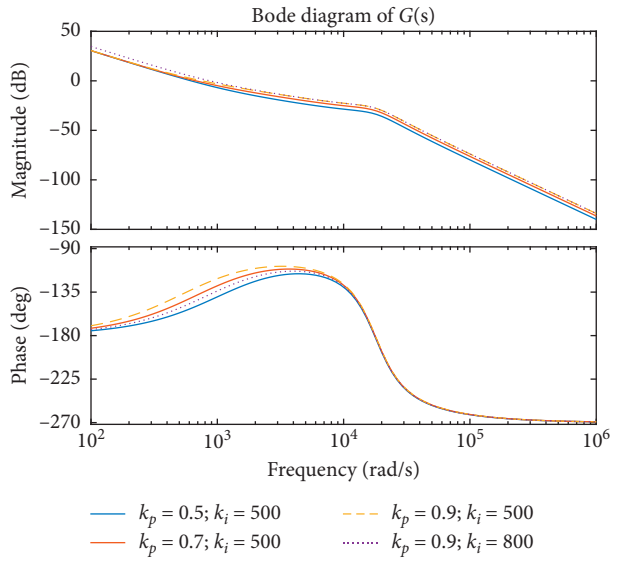

FIGURE 5: Under the different K_i and K_p, the system current is in the inner Bode diagram.

In order to make the system have good dynamic performance and robustness, it is necessary to ensure that P_M is in the (30°, 60°) range and G_M $(f_r) > 3$ dB (considering the 3 dB margin) is at the resonant frequency ω_r. Selecting the system's phase angle margin PM > 30°, H_{i1} needs to meet

$$P_M = 180^\circ + \angle G_{-0}(j2\pi f_c) \geq 30^\circ. \tag{6}$$

We bring the formula (1) into (7) and sort out

$$H_{i1} \leq \frac{A - B}{(2\pi f_c)^2 L_2 C K_{\text{pwm}}}, \tag{7}$$

where

$$A = \tan\left[-30^\circ + \arctan\left(2\pi f_c \frac{K_p}{K_i}\right)\right],$$
$$B = (2\pi f_c)^3 L_1 L_2 C + (2\pi f_c)(L_1 + L_2). \tag{8}$$

The amplitude margin G_M of the grid-connected system is

$$G_M = -20\log\left|G_{-0}(j2\pi f)_r\right| \geq 3\text{dB}. \tag{9}$$

We bring formula (1) into formula (9) and replace the PI controller $G_{\text{PI}}(s)$ with the proportional regulator K_P.

$$H_{i1} \geq \frac{10^{G_M/20} K_{\text{pwm}} K_{p1} \sqrt{L_1 L_2 C} L_1}{(L_1 + L_2)^{3/2} K_{\text{pwm}}}. \tag{10}$$

Reference [15] deduces the relationship between H_{i1} and system damping ratio ζ and the relationship between system damping ratio ζ and α:

$$H_{i1} \geq 2L_1 \zeta \sqrt{\frac{L_1 + L_2}{L_1 L_2 C}}, \tag{11}$$

$$\zeta > \sqrt{\frac{\left(1 - \sqrt{1 - 1/10^{1/5\alpha}}\right)}{2}}, \tag{12}$$

where $\alpha = f_c/f_r$. For the convenience of calculation, we ignored the filter capacitor branch and used a single L-type filter instead of the LCL filter. The current inner loop transfer function can be simplified as

$$G(s) \approx \frac{K_{\text{pwm}} K_{p1}}{s(L_1 + L_2)}. \tag{13}$$

Since the current inner loop gain is 1 at the cut-off frequency f_c,

$$\left|G(j2\pi f_c)\right| = 1 \approx \frac{K_{\text{pwm}} K_{p1}}{s(L_1 + L_2)}. \tag{14}$$

The relationship between f_c and K_P can be obtained as follows:

$$f_c \approx \frac{K_{p1} K_{\text{pwm}}}{2\pi(L_1 + L)_2}. \tag{15}$$

Bringing formulas (12) and (15) into formula (11), the capacitance current coefficient can be obtained H_{i1_ζ} under the constraint of damping ratio ζ:

$$H_{i1\_\zeta} > 2L_1 \sqrt{\frac{1 - \sqrt{1 - 1/10^{f_c/5f_r}}}{2}}. \tag{16}$$

If the parameter of K_p controller is adjusted due to operational requirements, the cut-off frequency f_c will also change, and a higher f_c value will promote the dynamic response of the system. Generally, the resonance frequency f_r is larger than the cut-off frequency f_c, so is the ratio α between [0, 1]. When the system damping is fixed, the smaller the α value, the better the damping effect of the system's resonance. When the cut-off frequency f_c is constant, the larger the damping ratio, the smaller the resonant peak.

As can be seen from the above, under the requirement of the phase margin and amplitude margin of the stable operation of the system, an appropriate value of H_{i1} can make the system show better dynamic response without affecting the steady state of the system. Therefore, the selection process for the current inner loop parameters K_p, K_i, and H_{i1} is as follows:

(1) Substitute the controller parameters K_P and K_i into formula (7) and (10) to obtain the value range $[H_{i1\_\min}, H_{i1\_\max}]$ of H_{i1}.

(2) Determine the cut-off frequency f_c of the system and substitute it into formula (16) to calculate H_{i1_ζ} under the condition of the damping ratio.

(3) Confirm whether the result of H_{i1_ζ} satisfies the range of H_{i1}. If it is satisfied, select the larger values between $H_{i1\_\min}$ and H_{i1_ζ}. Otherwise, select $H_{i1\_\min}$.

From the above analysis, the selection of the capacitive current feedback coefficient is affected by the controller parameters, so determining the appropriate PI parameters is very important for the system resonance damping.

5. Parameter Optimized Method Based on Particle Swarm Optimization to Optimize RBF

5.1. RBF Neural Network. Moody and Darken proposed the RBF neural network in 1989 and verified that the network has the best nonlinear approximation performance. RBF neural network has the advantages of fast learning speed and global approximation ability. Compared with BP neural network, it shows stronger universality and is widely used in various fields [16]. The RBF neural network is a three-layer feed-forward network, and its structure is shown in Figure 6.

Figure 6 shows a typical structure of an RBF neural network. The RBF network includes a signal input layer, an intermediate hidden layer, and an output layer. In the figure, $x = [x_1, x_2, \ldots, x_l]^T \in R^l$ is the network input vector, and $c_j = [c_1, c_2, \ldots, c_i, \ldots, c_m]^T$ is the data center vector of the RBF network hidden layer, $i = 1, 2, \ldots, n$. w_{ij} is the weight vector of the middle layer to the output layer. The network output is $y = [y_1, y_2, \ldots, y_n]^T$, and $\phi_j(*)$ is the radial basis function of the jth hidden node. The radial center network is symmetrical about the data center of the hidden layer, and the smaller the difference between the input signal and the data center, the higher the degree of the activation of this node, which is a local characteristic of the radial base network. Gaussian functions are often used as radial basis functions:

$$\phi_i(x) = \exp\left(-\frac{\|x - c_i\|^2}{2\sigma_i^2}\right), \tag{17}$$

where $i = 1, 2, \ldots, n$. $\sigma = [\sigma_1, \sigma_2, \ldots, \sigma_m]^{\mathrm{T}}$ is called the basis function width or expansion coefficient, which means that different function values are calculated under the same input data and data center distance.

Therefore, for an RBF network, each node of the hidden layer will have its own corresponding data center. It can be seen from Figure 6 that the output of the kth output node of the RBF network can be expressed as

$$y_k = \sum_{j=1}^{m} w_{ij}\phi_j\left(\|x - c_j\|, \sigma_j\right), \tag{18}$$

where the input vector x is consistent with the dimension of c_j.

5.2. Particle Swarm Optimization for RBF. The conventional gradient descent training method of the RBF network is easy to fall into a local optimum, so the initial value of the network parameters will affect the identification of the PI parameter values. Therefore, this paper uses particle swarm optimization (PSO) to optimize the network. Particle swarm optimization is one of the most mature and widely used adaptive probability search optimization algorithms in evolutionary algorithms [17, 18]. A flow chart for optimizing the initial weight of the RBF neural network based on the particle swarm optimization is shown in Figure 7.

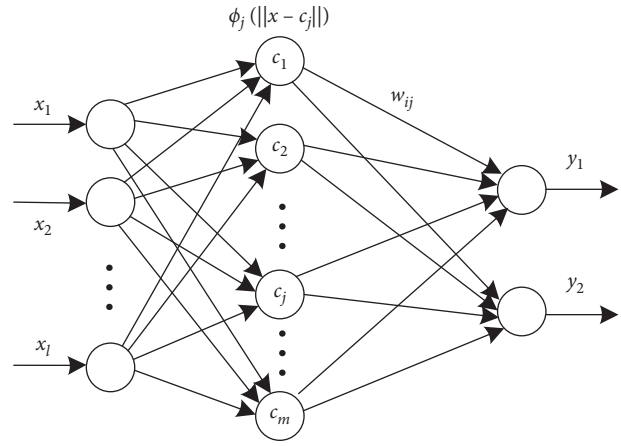

Figure 6: RBF neural network structure.

The fitness function of the particle swarm optimization uses the error function to calculate the individual fitness:

$$E = \frac{1}{L}\sum_{j=1}^{L}\sum_{k=1}^{p}\left(d_{jk} - y_{jk}\right)^2, \tag{19}$$

where y_{jk} is the actual output of the neuron k corresponding to the j_{th} sample input and d_{jk} is the expected output of the neuron k.

The PSO optimize RBF neural network process is as follows:

(1) Determine the initial population. The data center c_i, the expansion coefficient σ, and the weight W_j population size are determined according to the network structure.

(2) Encode individuals. In this paper, the data center c_i and the expansion constant are arranged in a cross, and the weight is placed at the back. Among them, the data center c_i and the extended constant have a value range of [−8, 8], and the weight value ranges from [−1, 1].

(3) Update the speed and position of particles.

(4) Evaluate the fitness function. If the requirements are met, go to (5); otherwise, go to (3) to continue execution.

(5) Assign the optimized parameters to the RBF neural network.

5.3. Neural Network Controller Optimization. The adaptive resonance suppression control strategy proposed in this paper is based on the addition of an adaptive correction link on the control system using a PI controller. This method does not increase the complexity of the control system and can timely correct the control parameters of the control system according to the change of the impedance of the power grid.

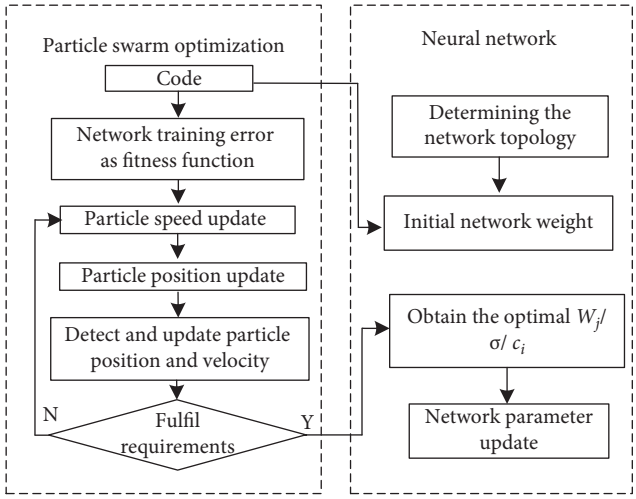

Figure 7: Schematic diagram of particle swarm optimization RBF network.

The block diagram of the control structure using the RBF neural network is shown in Figure 8; it includes two main components: the PI self-correction link and the particle swarm optimization-optimized RBF network.

In the working process of the system, the RBF network based on particle swarm optimization is mainly used to adjust the error signal. As shown in Figure 8, the RBF network element has two inputs: the grid-connected current and the output signal of the PI controller, which can be expressed as follows: $x = [x_1\ (k)\ x_2\ (k)]^T = [u\ (k-1)\ i_{2d}\ (k-1)]^T$. When the impedance of the grid changes and the system is disturbed, the ideal tracking signal $y_m\ (k)$ is obtained through the identification capability of the RBF itself. So, the output of the RBF network can be expressed as

$$y_m(k) = w_1 h_1 + w_2 h_2 + \cdots + w_m h_m. \tag{20}$$

The expression of the difference value $e\ (k)$ between the grid-connected current $i_{2d}\ (k)$ and the output $y_m\ (k)$ of the network is

$$e(k) = y_m(k) - i_{2d}(k). \tag{21}$$

The error indicators of the learning weight of the RBF network are

$$E(k) = \frac{1}{2} e(k)^2. \tag{22}$$

The extension coefficient $\sigma_j\ (k)$, the node data center $c_j\ (k)$, and the output weight $W_j\ (k)$ of the network are updated based on the particle swarm optimization method to ensure the tracking performance of the RBF network. A correction information matrix for grid-connected current input to the RBF neural network can be derived:

$$\frac{\partial i_{2d}(k)}{\partial u(k)} \approx \frac{\partial y_m(k)}{\partial u(k)} = \sum_{j=1}^{m} w_j(k) h_j \frac{C_{ji} - u(k)}{\sigma_j^2}. \tag{23}$$

The Jacobian information matrix is sent to the PI self-controller to correct the PI controller parameters. Definition error e_c is

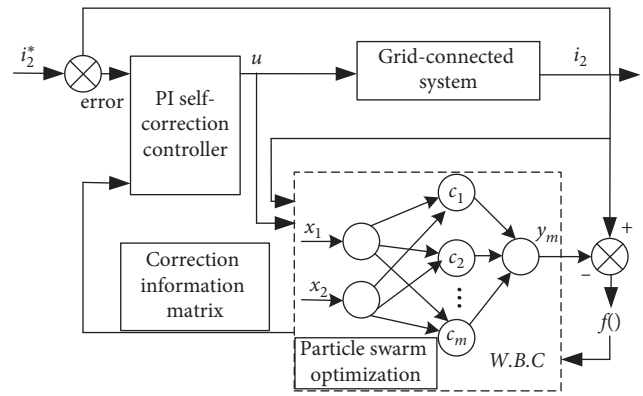

Figure 8: Block diagram based on PSO_RBF network adaptive controller.

$$e_c(k) = i_{2d}^*(k) - i_{2d}(k), \tag{24}$$

k_p and k_i values can be expressed as

$$\begin{cases} K_p(k) = K_p(k-1) + \Delta K_p(k) + \partial_c \left[K_p(k-1) - K_p(k-2)\right], \\ K_i(k) = K_i(k-1) + \Delta K_i(k) + \partial_c \left[K_i(k-1) - K_i(k-2)\right], \end{cases} \tag{25}$$

where ∂_c is the momentum factor; η is the learning rate; $\Delta K_p\ (k)$ and $\Delta K_i\ (k)$ are expressed as follows:

$$\begin{cases} \Delta K_p = \eta e_c(k) \dfrac{\partial i_{2d}(k)}{\partial u(k)} \left[e_c(k) - e_c(k-1)\right], \\ \Delta K_i = \eta e_c(k)^2 \dfrac{\partial i_{2d}(k)}{\partial u(k)}. \end{cases} \tag{26}$$

Therefore, the output of the PI self-correction controller is

$$u(k) = u(k-1) + K_i e_c(k) + K_p \left[e_c(k) - e_c(k-1)\right]. \tag{27}$$

6. Simulation Analysis

In order to verify the effectiveness of the method presented in this paper, the controller parameters were adjusted using the RBF network method and PSO_RBF network method when the impedance of the power grid is changed. The inverter uses the SPWM method, and the system parameters are shown in Table 1. In order to ensure stable operation, it is required that the phase angle margin PM be greater than 30° and the amplitude margin GM be greater than 3 dB of the grid-connected system. The parameters of the PI controller of the system after particle swarm optimization are $k_p = 0.45$ and $k_i = 500$.

Figure 9 shows a Bode plot of the loop gain of the system with different controllers. As shown in the figure, $G_0\ (s)$ is the Bode diagram with the system working normally, $G_1\ (s)$ is the Bode diagram with the grid impedance being increased to 1.2 mH, and $G_2\ (s)$ and $G_3\ (s)$ are Bode diagrams using RBF network PI controller and PSO_RBF network PI controller, respectively. From the Bode diagram of $G_1\ (s)$, it can be known that when the grid impedance is

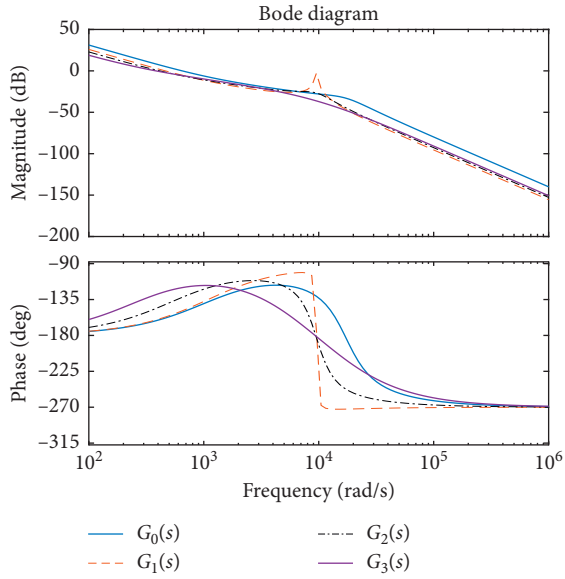

Figure 9: Board diagram of system loop gain under different controllers.

increased to 1.2 mH, the system controller parameters and capacitor current feedback parameters do not adapt to the new grid impedance, which leads to new resonances and causes the system's instability. $G_2(s)$ is the Bode diagram of the system with the PI parameters being set using the RBF neural network; in this case, the PI controller parameters are adjusted to $K_p = 0.64$ and $K_i = 350$, the resonance peak of the system is suppressed, and the stability margin of the system is 25 dB (33°). $G_3(s)$ is the Bode diagram of the system with the PI parameters being set using the PSO_RBF neural network; in this case, the PI controller parameters are adjusted to $K_p = 0.8$ and $K_i = 210$, the resonance problem peak of the system has been improved, and the stability margin is 40 dB (48°), which ensures the stability of the system's operation.

We set the experimental parameters according to the parameters in Table 1, increase the grid inductance $L_g = 1.2$ mH at 1 s, and observe the change waveform of the grid-connected current as shown in Figure 10. It can be seen from the figure that, with the grid impedance changes, the grid-connected current is significantly distorted and contains harmonics, which affects the current quality.

In the case of grid impedance changes, we use the RBF network and PSO_RBF network to optimize the controller parameters and then update the capacitor current feedback coefficient. Grid-connected system simulation is performed through SIMULINK, and the results are compared and analysed.

In Figure 11 , using the PI controller with parameters is adjusted by the RBF neural network at 0.2 seconds. According to FFT analysis, this method can reduce system harmonics caused by changes in grid impedance. Total harmonic distortion (THD) of grid current is reduced to 2.17%, and grid-connected current is 16.82 A which is less than the reference current of 17 A.

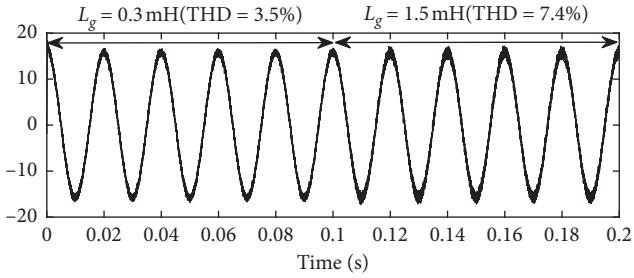

Figure 10: Current waveform when the grid resistance changes at 0.1 s.

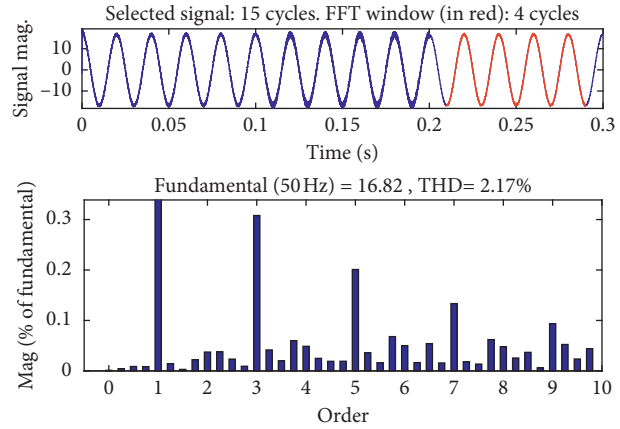

Figure 11: Grid-connected current when RBF optimizes parameters.

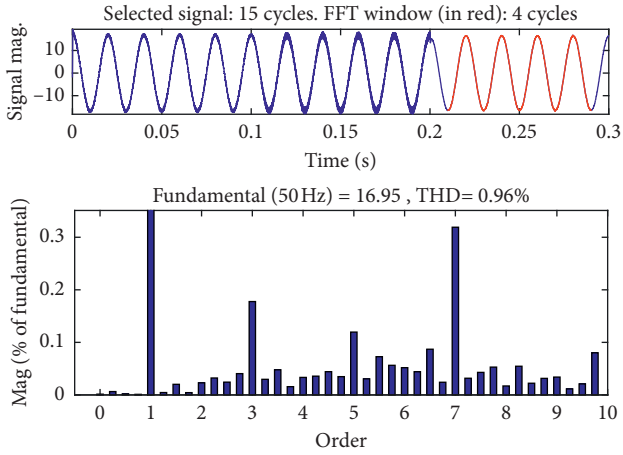

Figure 12: Grid-connected current under PSO_RBF optimization parameters.

Figure 12 shows the FFT analysis of the grid-connected current with the PI controller parameters being adjusted by the PSO_RBF method. After the PSO_RBF network has adjusted the controller parameters and updates the capacitor current feedback coefficient, the grid-connected current changes significantly at 0.2 seconds. From the FFT analysis, it can be seen that this method can be used to suppress system harmonics caused by grid impedance changes. In this case, the THD of the grid-connected current is only 2.17%, the

grid-connected current value is 16.95, and the error between grid current and reference current t is small. This method can ensure a good improvement in the quality of the grid-connected current.

The comparison of simulation results shows that the adaptive PI controller based on the PSO_RBF neural network has good adjustment performance. When the grid impedance changes, it can quickly find the suitable controller parameter value to make the system grid-connected current stable. Based on the constraint conditions such as stability margin and damping ratio, the capacitance current feedback coefficient is calculated; this can effectively suppress system resonance and reduces grid-connected current ripple.

7. Discussion and Conclusions

This paper conducts a study on the resonance problem of LCL-type grid-connected converter, and the generation and suppression of resonance are systematically analysed. The main research results are as follows:

(1) This paper conducts an impedance model based on a single-phase converter and analysis system resonance. It reaches the conclusion that the LCL grid-connected converter is affected by the impedance of the grid and the system resonance changes. An adaptive control strategy based on the PAO_RBF network is proposed, in which the controller parameters can be adjusted quickly and accurately according to the change of the grid impedance. This method effectively reduces system steady-state error.

(2) Based on the results of resonance analysis, the effectiveness of using capacitor current feedback to suppress resonance is pointed out. In order to solve the system resonance problem caused by the impedance change of the power grid, this paper uses particle swarm optimization to optimize the RBF network to adjust PI controller parameters and calculates the capacitor current feedback coefficient under the constraints of the system's stability margin and damping ratio. By comparing it with the RBF neural network optimization method, it can be seen that the PAO_RBF method can effectively make the control parameters adjust with the change of the grid impedance in time, thus, more effectively suppressing the system resonance.

Data Availability

The data used to support the findings of this study are available from the corresponding author upon request.

Conflicts of Interest

The authors declare no conflicts of interest.

Acknowledgments

This research was supported in part by the Natural Science Foundation of Ministry of Education of Guizhou Province under Grant nos. [2019]071 and [2019]205, the Nature Science Foundation of Qiannan under Grant no. [2018]05, and the Science and Technology Foundation of Guizhou Province under Grant no. [2019]1447 and LH[2017]7231.

References

[1] B. Zeng, J. Zhang, X. Yang, J. Wang, J. Dong, and Y. Zhang, "Integrated planning for transition to low-carbon distribution system with renewable energy generation and demand response," *IEEE Transactions on Power Systems*, vol. 29, no. 3, pp. 1153–1165, 2014.

[2] X. Liu, P. Ma, G. He, and D. Wang, "Study on control strategy of LCL type single-phase grid-connected inverter," in *Proceedings of the 2018 3rd International Conference on Mechanical, Control and Computer Engineering (ICMCCE)*, pp. 37–42, Huhhot, China, September 2018.

[3] X. F. Wan, X. Y. Nie, Z. P. Liao, X. H. Ding, and F. P. Zeng, "Resonance damping method of single-phase inverter with LCL-filter based on error signal feedback," *Electric Machines and Control*, vol. 22, no. 5, pp. 102–109, 2018.

[4] L. M. Zhou, A. Luo, Y. D. Chen, and Z. Y. Chen, "A single-phase grid-connected power control and active damping optimization strategy with LCL filter," *Transactions of China Electrotechnical Society*, vol. 31, no. 6, pp. 144–154, 2016.

[5] B. Q. Liu, H. Guo, and Y. X. Zhu, "Analysis and design of a passively damping LCL filter in three-phase converters," *Transactions of China Electrotechnical Society*, vol. 32, no. 2, pp. 195–205, 2017.

[6] C. Chen, J. Xiong, Z. Wan, J. Lei, and K. Zhang, "A time delay compensation method based on area equivalence for active damping of an LCL -type converter," *IEEE Transactions on Power Electronics*, vol. 32, no. 1, pp. 762–772, 2017.

[7] T. Liu, J. Liu, Z. Liu, and Z. Liu, "A study of virtual resistor-based active damping alternatives for LCL resonance in grid-connected voltage source inverters," *IEEE Transactions on Power Electronics*, vol. 35, no. 1, pp. 247–262, 2020.

[8] Z. Miao, S. Long, W. Yao, and Z. Lu, "A self-tuning notch filter based hybrid active damper for LCL-type grid-tied inverters with adaptability to weak grids," in *Proceedings of the 2019 10th International Conference on Power Electronics and ECCE Asia (ICPE 2019-ECCE Asia)*, pp. 2970–2977, Busan, South Korea, May 2019.

[9] J. Hu, J. Zhu, and D. G. Dorrell, "Model predictive control of inverters for both islanded and grid-connected operations in renewable power generations," *IET Renewable Power Generation*, vol. 8, no. 3, pp. 240–248, 2014.

[10] K. Seifi and M. Moallem, "An adaptive PR controller for synchronizing grid-connected inverters," *IEEE Transactions on Industrial Electronics*, vol. 66, no. 3, pp. 2034–2043, 2019.

[11] W. J. MA, S. OuYang, and L. Yang, "A new resonant control strategy for three-phase grid connected inverter," *Power System Technology*, vol. 43, no. 8, pp. 2884–2891, 2019.

[12] G. Pandove and M. Singh, "Robust repetitive control design for a three-phase four wire shunt active power filter," *IEEE Transactions on Industrial Informatics*, vol. 15, no. 5, pp. 2810–2818, 2019.

[13] E. Durna, "Adaptive fuzzy hysteresis band current control for reducing switching losses of hybrid active power filter," *IET Power Electronics*, vol. 11, no. 5, pp. 937–944, 2018.

[14] C. L. Bao, X. B. Ruan, X. H. Wang, and D. H. Pan, "Design of grid-connected inverters with LCL filter based on PI regulator and capacitor current feedback active damping," *Proceedings*

of the Chinese Society for Electrical Engineering, vol. 32, no. 25, pp. 133–142, 2012.

[15] Y. C. Lü, H. Lin, H. C. Yang, and Y. Luo, "Decouple design of current loop parameters for PWM converters based on multi-resonant controllers and capacitor current feedback active damping," *Proceedings of the CSEE*, vol. 33, no. 27, pp. 44–515, 2013.

[16] W. Yang, J. Guo, Y. Liu, and G. Zhai, "Multi-objective optimization of contactor's characteristics based on RBF neural networks and hybrid method," *IEEE Transactions on Magnetics*, vol. 55, no. 6, pp. 1–4, 2019.

[17] J.-S. Yang, Y.-W. Chen, and Y.-Y. Hsu, "Small-signal stability analysis and particle swarm optimisation self-tuning frequency control for an islanding system with DFIG wind farm," *IET Generation, Transmission & Distribution*, vol. 13, no. 4, pp. 563–574, 2019.

[18] A. A. Abou El-Ela, M. Kamal, T. Fetouh, and R. A. Amer, "Partical swarm optimization tuning based controlled series FACTS for power system stability enhancement," in *Proceedings of the 2019 21st International Middle East Power Systems Conference (MEPCON)*, pp. 939–945, Cairo, Egypt, 2019.